ORIGINAL PAPER - EXPLORATION GEOLOGY

Fluid inclusion characteristics of the Jurassic reservoir and hydrocarbon accumulation process in the eastern Kuqa Depression, Tarim Basin

Jialin Wan[1,2] · Yanjie Gong[2] · Qingong Zhuo[2] · Xuesong Lu[2] · Wenhui Huang[1]

Abstract

There has been significant progress in hydrocarbon exploration of the eastern Kuqa Depression, Tarim Basin, whose Jurassic reservoir is a key area for abundant hydrocarbon with poorly understood accumulation mechanism. This study conducts an integrated investigation comprising petrographic observations, microthermometry measurements, and fluorescence spectroscopy analyses on fluid inclusions to reconstruct hydrocarbon accumulation history in the Jurassic reservoir. These conclusions are combined with biomarker characteristics to reveal the burial history and thermal evolution of the study area. The results show that (1) there were two episodes of oil charging that occurred at 6~4 Ma and 4~2 Ma, respectively. The QGF experiment response and yellow fluorescent oil inclusions indicated that low-maturity medium crude oil from the Triassic source rocks was expelled into the upper Ahe Formation. In the second charging stage, some mature oil generated from Jurassic source rocks was charged into the reservoir of the Kezilenuer and Yangxia formations, while the condensate from the Triassic source rocks was migrated upward to the Jurassic reservoir, consistent with smaller QGF-E intensity values and blue-white fluorescent petroleum inclusions. (2) There were two kinds of hydrocarbon accumulation models including the lower-generation and upper-storage and the self-generated and self-stored models. (3) It was noted that active faults were developed under the compression stress to provide channels for hydrocarbon vertical migration. Moreover, the early reservoir was destroyed resulting from the strata denudation and a large amount of crude oil was escaped to the surface. The findings of this study can help for better understanding of hydrocarbon accumulation mechanism in the eastern Kuqa Depression and provide theoretical guidance for further oil and gas exploration.

Keywords Tarim Basin · Kuqa Depression · Fluid inclusions · Accumulation history · Biomarker characteristics

Abbreviations

GC–MS	Gas chromatography-mass spectrometry
QGF	Quantitative grain fluorescence
QGF-E	Quantitative grain fluorescence on extract
Th	Homogenization temperature
TT	Tricyclic terpane
ST	Regular sterane
λ max	Maximum fluorescence emission wavelength
pc	Photometer count
POWC	Paleo-oil–water contact

✉ Yanjie Gong
2287239371@qq.com

1   School of Energy Resources, China University of Geosciences (Beijing), Beijing 100083, China

2   Research Institute of Petroleum Exploration and Development, PetroChina, Beijing 100083, China

Introduction

The hydrocarbon accumulation mechanism has always been an important scientific issue for geologists (Anees et al. 2019, 2022). The charging process of oil and gas in hydrocarbon-bearing basins is complex, and, therefore, it is important to comprehensively analyze the accumulation characteristics to aid oil and gas exploration (Zhao et al. 2004). The analysis of fluid inclusions is a new method to investigate oil and gas accumulation process (Chen et al. 2000). Fluid inclusions have become a hot topic within hydrocarbon basin research, because it not only contains abundant information of accumulation and mineralization, but also provides

indications on the oil and gas accumulation and resource evaluation or exploration (Burruss et al. 1983; Haszeldine et al. 1984a; Parnell 2010; Guo et al. 2016a). When petroleum is expelled into the reservoir, some fluid inclusions of the rock-forming and ore-forming components are captured by the cement and micro-fractures during the process of mineral crystallization, and these inclusions record information on fluid temperature, pressure, and composition during oil and gas migration (Chen et al. 2000; Parnell et al. 2010). The geological properties of hydrocarbon inclusions and brine inclusions contain important information on migration and accumulation and help in the study of hydrocarbon accumulation chronology (Horsfield et al. 1984; Goldstein 2001; Liu et al. 2013; Thanh et al. 2020; Thanh et al. 2022). Investigations of fluid evolution in petroliferous basins are critical for understanding petroleum migration and accumulation and have significance for predicting the distribution of hydrocarbon resources (Guo et al. 2016b; Thanh et al. 2019). The Kuqa Depression is rich in oil and gas resources and regarded as a key area for hydrocarbon exploration (Wei and Jia 1998; Qin et al. 2002; He et al. 2004; Jia and Li 2008). The depression has widely distributed and thick coal measures strata, with rich gas source rocks containing abundant organic matter (Dai et al. 2012).

Previous studies have shown that the Kuqa Depression has significant geological features to enable multi-source hydrocarbon supply, multi-phase charging and late accumulation (Ma et al. 2003; Zhu et al. 2012; Guo et al. 2016b, 2018). It is generally believed by most scholars that natural gas charging has occurred in the Kuche stage, and the reservoir formed in the early stage has suffered structural destruction and adjustment in the late (Zhao and Dai 2002; Li et al. 2013). However, there are some differences regarding the sources and charging periods of crude oil. Some scholars think that there is only one stage of oil charging in the Kuqa Depression, which is contributed by Triassic lacustrine mudstone (Zhao and Lu 2003; He et al. 2013; Li et al. 2016). Others believe that there is not only the lacustrine oil charging but also the second stage oil migration caused by the Jurassic coal measure source rocks (Zhao and Dai 2002; Wu et al. 2016b; Zhao et al. 2019). We find that the predecessors only take multiple sets of fluid inclusions analyses or source rocks and crude oil biomarker compound comparison for the research of hydrocarbon accumulation, which restricts the comprehensive geological understanding of the hydrocarbon exploration potential in the Kuqa Depression. Therefore, our study investigates the geochemical characteristics of fluid inclusions combined with the biomarker compounds of crude oil to discuss hydrocarbon accumulation mechanism of Jurassic reservoir in the eastern Kuqa Depression systematically.

In this study, we take the Jurassic reservoir of Well MN1 in the eastern Kuqa Depression as the research object

and focus on three scientific issues: (1) which source rocks produced petroleum; (2) when the hydrocarbon was charged into the reservoir; and (3) when the hydrocarbon reservoir was formed. Firstly, the geological setting is present. Then, the sample preparation and the operation flow of different experimental methods are introduced. Thirdly, experimental results are showed and discussed to analyze the hydrocarbon accumulation mechanism. Moreover, the core samples are divided into three parts for experimental testing (Fig. 1). Gas chromatography-mass spectrometry (GC–MS) analysis is used to analyze the biomarker characteristics of saturated hydrocarbon for oil-source correlation identification, to identify the contribution of different types of organic matter, and to determine the sedimentary environment. Observations of the petrographic characteristics and homogenization temperature measurements for fluid inclusions are conducted to identify the different charging periods and determine the time of hydrocarbon migration for each phase based on the burial history and thermal evolution of the source rocks. The fluorescence spectroscopy analyses can indicate the development of hydrocarbon reservoir in the Jurassic strata. This study aims to establish the Jurassic hydrocarbon accumulation model in the eastern Kuqa Depression, update the understanding of oil and gas geology, and provide theoretical
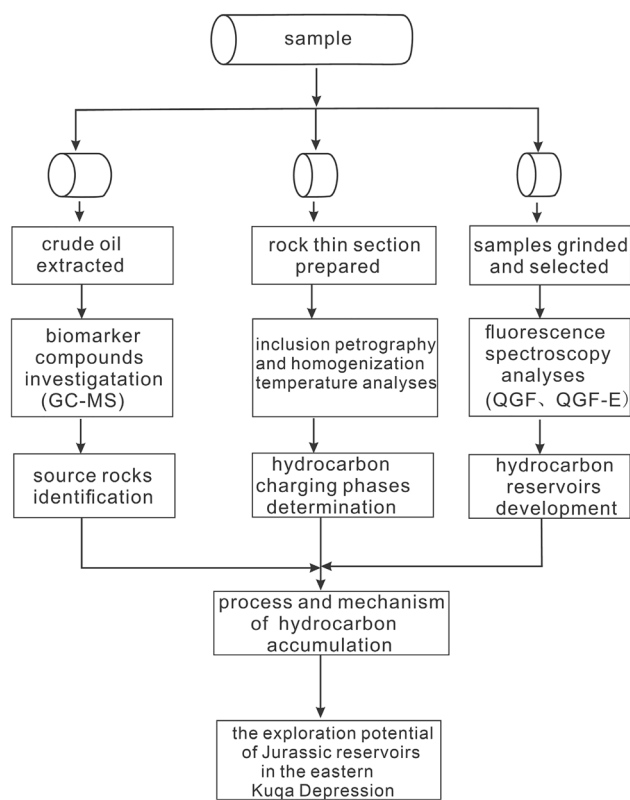

Fig. 1 Flowchart of experiment and analysis of geological problems

guidance for further petroleum exploration and development in the study area.

Geological settings

The Tarim Basin is a superimposed basin and the area with the largest oil and gas resources in Northwest China (Guo et al. 2016a) (Fig. 2A). The Kuqa Depression, as a Mesozoic-Cenozoic basin, has abundant oil and gas resources and covers an area of 37,000 km² (Jia 2003) (Fig. 2B). The depression is a regenerated foreland basin and divided into four belts and three sags (He et al. 2005; Wu et al. 2016a) (Fig. 2C). The north-dipping and nearly EW-trending Yiqikelike fault is developed in the Triassic to Palaeogene strata and has played an important role in the distribution

of gas reservoirs (Wei et al. 2016). The study area in this work is located in the Tugerming area, which is to the west of the Yiqikelike tectonic belt (Fig. 2C). The accurate interpretation of clutter seismic reflection data and drilling data from previous research show that the Ahe Formation has been drilled in the study area and the Jidike Formation is in an unconformable contact with the Jurassic strata in well MN 1 (Chai et al. 2020) (Fig. 2D).

The Kuqa Depression is a terrigenous clastic deposit dominated by Mesozoic and Cenozoic sediments with a thickness of over 8000 m (Qin et al. 2002). During the Late Triassic ~ Middle Jurassic, thick lacustrine and lacustrine-marsh source rocks were deposited in the Kuqa Depression under a warm and humid climate (Zhao and Zhang 2002). The source rocks of the Mesozoic strata are characterized by large thickness and wide distribution, a high

Fig. 2 A Map showing the location of the Tarim Basin in China; B location map showing the tectonic units of the Tarim Basin and the Kuqa Depression adjacent to the South Tianshan Mountains; C distribution of the tectonic units in the Kuqa Depression and the location of well MN 1 in the Yiqikelike thrust belt; D cross-section AB showing the stratigraphic distribution in Well MN 1 in the eastern Kuqa Depression (Modified from Chai et al. (2020))
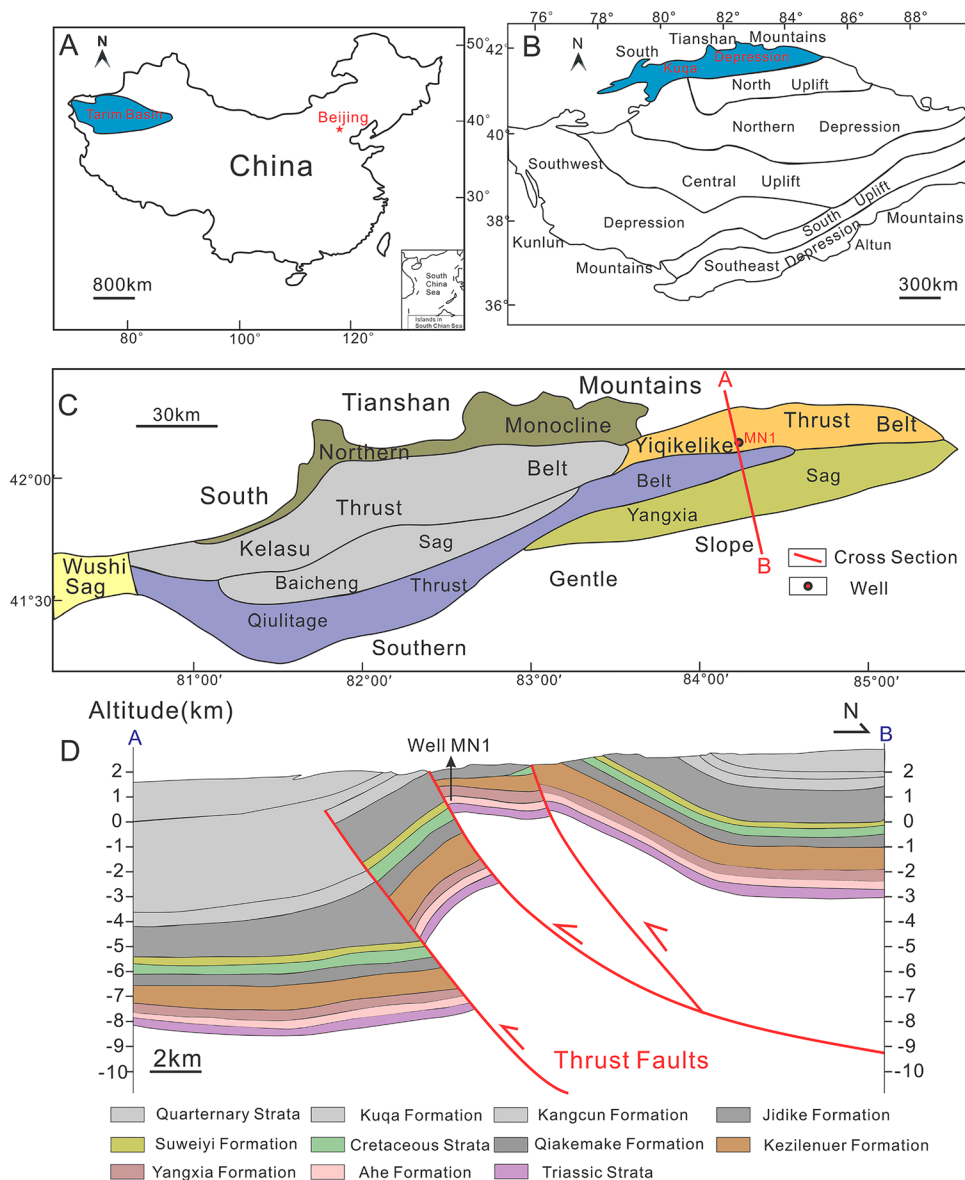
abundance of organic matter, and high maturity. They are composed of three sets of lacustrine source rocks and three sets of coal source rocks (Du et al. 2006; He et al. 2013) (Fig. 3). Moreover, the Lower Jurassic reservoir's rock types are dominated by lithic sandstones with medium sorting, subrounded-subangular grinding, and low cement content with primary intergranular pores and intergranular dissolved pores, a small amount of intragranular dissolved pores, and fractures (Ju et al. 2014).

There are two sets of source-reservoir assemblages in the eastern Kuqa Depression: (1) the oil and gas generated from the Lower Triassic strata were migrated upward to the reservoir of the Ahe Formation, and sealed by the coal measures strata at the bottom of the Yangxia Formation; (2) hydrocarbon generated from the source rocks of the Yangxia Formation were stored in situ and sealed by the upper mudstone

(Ju et al. 2014). The tight contact relationship between the source-reservoir-cap assemblages developed in the eastern Kuqa Depression improved the efficiency of hydrocarbon expulsion, which was beneficial to the hydrocarbon accumulation in the tight sandstone reservoir.

Samples and methods

There are 24 sandstone samples from Well MN 1 of the Tugerming area in the eastern Kuqa Depression (Fig. 2C). These samples are selected from the depth interval of 417.2~1154.6 m, including 6 from the Kezilenuer Formation (J_2kz), 3 from the Yangxia Formation (J_1y), and 15 from the Ahe Formation (J_1a). Their basic information and lithological features are listed in Table 1.

Fig. 3 Comprehensive columnar map of the strata and the major petroleum system elements in the eastern Kuqa Depression. Modified from Guo et al. (2016a)
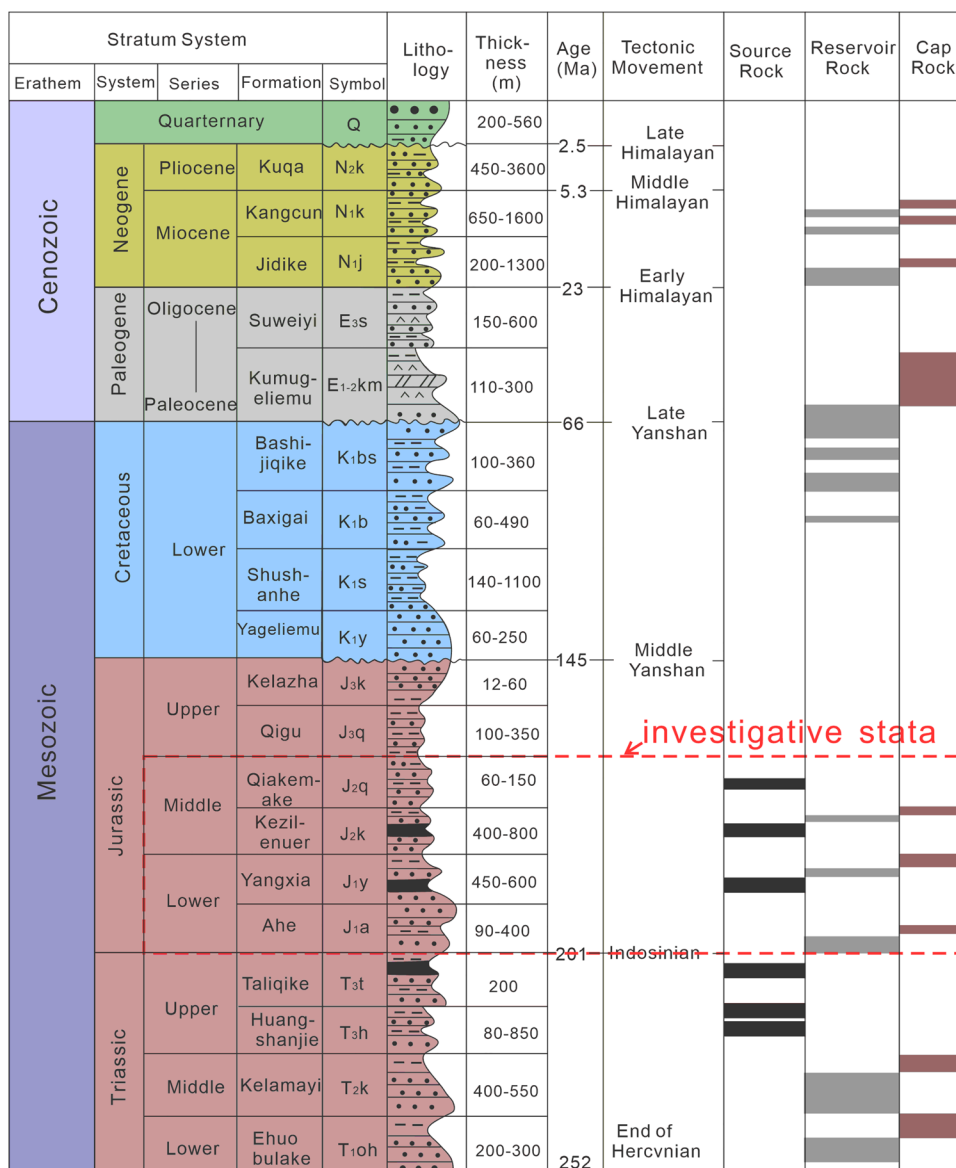
Table 1 Characteristics of the core samples analyzed in the study

Sample No	Depth/m	Formation	Lithology	Type	Analysis
MN1-1	417.2	J$_2$kz	Medium sandstone	Core	PM, GC–MS, QFT
MN1-2	418.6	J$_2$kz	Medium coarse sandstone	Core	GC–MS, QFT
MN1-3	421.0	J$_2$kz	Siltstone	Core	GC–MS, QFT
MN1-4	603.5	J$_2$kz	Sandy conglomerate	Core	PM, GC–MS, QFT
MN1-5	604.7	J$_2$kz	Sandy conglomerate	Core	GC–MS,QFT
MN1-6	607.5	J$_2$kz	Sandy conglomerate	Core	GC–MS,QFT
MN1-7	777.6	J$_1$y	Sandy conglomerate	Core	GC–MS,QFT
MN1-8	780.0	J$_1$y	Sandy conglomerate	Core	GC–MS,QFT
MN1-9	781.9	J$_1$y	Coarse sandstone	Core	GC–MS,QFT
MN1-10	951.7	J$_1$a	Medium sandstone	Core	PM,GC–MS,QFT
MN1-11	954.8	J$_1$a	Medium sandstone	Core	QFT
MN1-12	963.9	J$_1$a	Medium coarse sandstone	Core	PM,GC–MS,QFT
MN1-13	967.3	J$_1$a	Coarse sandstone	Core	GC–MS,QFT
MN1-14	970.8	J$_1$a	Coarse sandstone	Core	QFT
MN1-15	1024.6	J$_1$a	Coarse sandstone	Core	GC–MS,QFT
MN1-16	1029.0	J$_1$a	Coarse sandstone	Core	GC–MS,QFT
MN1-17	1032.2	J$_1$a	Sandy conglomerate	Core	PM,QFT
MN1-18	1034.8	J$_1$a	Coarse sandstone	Core	PM,GC–MS,QFT
MN1-19	1036.4	J$_1$a	Coarse sandstone	Core	GC–MS,QFT
MN1-20	1081.3	J$_1$a	Sandy conglomerate	Core	PM,GC–MS,QFT
MN1-21	1084.5	J$_1$a	Conglomerate	Core	GC–MS,QFT
MN1-22	1147.9	J$_1$a	Sandy conglomerate	Core	QFT
MN1-23	1150.7	J$_1$a	Sandy conglomerate	Core	QFT
MN1-24	1154.6	J$_1$a	Medium sandstone	Core	PM,QFT

J2kz Kezilenuer Formation; *J1y* Yangxia Formation; *J1a* Ahe Formation; *PM*=petrographic observation and microthermometric measurement, *GC–MS* gas chromatography–mass spectrometry technique; *QGT* quantitative fluorescence technique referring to the quantitative grain fluorescence (QGF) and QGF on extract (QGF-E)

Systematic experimental analyses were adopted to study the hydrocarbon accumulation characteristics of the Jurassic strata, including gas chromatography-mass spectrometry (GC–MS), fluid inclusion analyses (petrographic observations and microthermometric measurements), and fluorescence spectroscopy (QGF and QGF-E). All experiments were conducted at the Key Laboratory of Basin Structure and Hydrocarbon Accumulation, CNPC, Beijing.

Gas chromatography-mass spectrometry (GC–MS)

The saturated hydrocarbon in the samples was eluted with n-hexane, toluene, and chloroform. They were then extracted by column chromatography followed by deasphalting with n-hexane. Gas chromatography–mass spectrometry analysis was systematically conducted on the extracted saturated hydrocarbon. The tricyclic terpanes and regular steranes were detected on the *m/z* 191 and 217 mass chromatogram, respectively. The GC–MS analysis was conducted with an ISQ 7000 single-quad mass spectrometer coupled to a Trace 1310 gas chromatograph equipped with an HP-5MS capillary column (60 m×0.25 mm i.d., film thickness 0.25 μm).

The oven temperature was initially set at 60 °C and programmed to 260 °C at a heating rate of 6 °C/min, and then increased to 320 °C at a rate of 1.5 °C/min and then persisted for 20 min. The mass spectrometer was operated in the full scan mode at an ionization energy of 70 eV and a source temperature of 310 °C. Helium was used as the carrier gas.

Fluid inclusion analyses

Doubly polished sections of approximately 100 mm in thicknesses were prepared from the five core samples for fluid inclusion petrographic analyses and microthermometric measurements. Additionally, all sandstone samples were disaggregated into individual grains by physical crushing (diameters of 0.063~1 mm) for the fluorescence spectroscopy analyses, including quantitative grain fluorescence (QGF) and QGF on extracts (QGF-E) analyses.

Petrographic observations of fluid inclusions

The thin sections were put under a Zeiss Axiovert 200 microscope equipped with both transmitted light and incident

ultraviolet light (UV) sources ($\lambda = 365$ nm) to observe the distribution, shape, size, phase state, color, and fluorescence of the fluid inclusions. Most fluid inclusions had a clear-cut outer boundary observed at room temperature using a transmitted light microscope due to the difference in the refractive index between the host mineral and the fluid inclusion (Jayanthi et al. 2020). With maturity increasing, the composition of the hydrocarbon inclusions changed from heavy oil through to medium oil and light oil and then to gas, which was coincident with a change in color from black or brown to tan, yellow, light yellow, and finally gray or colorless, and a further change in fluorescence colors from dark brown to brown, tan, yellow, yellow-green, blue-green, blue-white, and finally blue (Goldstein 2001).

Microthermometry measurements of the fluid inclusions

The principle and condition of the homogenization temperature measurements of the fluid inclusions were that the captured fluid was a uniform single-phase and closed system with constant volume characteristics (Liu and Gu 1997). The fluid inclusions were first heated at 10 °C/min until the phase boundaries disappeared. The homogenization temperatures (Th) of the fluid inclusions were then subsequently determined using a calibrated Linkam TH-600 stage apparatus. The results had a precision of ± 1 °C.

In this study, we used the PetroMod basin simulation software to simulate the burial history of Well MN 1. Previous results on the terrestrial heat flow value in the Kuqa Depression (Wang et al. 2005) and the model of vitrinite reflectance proposed by Burnham and Sweeney (1989) were used to reconstruct the thermal evolution of the well in this study.

Fluorescence spectroscopy analyses

Fluorescence spectroscopy analyses were conducted on a Varian Cary-Eclipse fluorescence spectrophotometer. The fluorescence intensity and spectral characteristics were identified to distinguish the geochemical information of the hydrocarbon inclusions adsorbed on the surface of the reservoir or inside the particles to identify and discuss the paleo/current oil–water interface and reservoir properties (Liu and Eadington 2005; Liu et al. 2007). Heavy minerals and cuttings were then removed by magnetic separation before the remaining grains were placed in a beaker and rinsed sequentially with a dichloromethane (DCM): methanol mixture (50:50), 30% hydrogen peroxide, and finally 3.6% dilute hydrochloric acid to remove free hydrocarbons, adsorbed hydrocarbons, and mineral impurities. Details of the approaches and methods used are given in Liu and Eadington (2005). The methods used a highly sensitive spectrophotometer to analyze ~ 1 g of clean, dry, whole

quartz grains in bulk volume (QGF) and the solvent extract (QGF-E) after a pre-cleaning procedure removed the surface contaminants.

Results

Characteristics of the biomarker compounds

Saturated hydrocarbon extracted from the Jurassic core samples was subject to GC–MS analysis to qualitatively and quantitatively identify the characteristics of the biomarkers. A series of tricyclic terpane and regular sterane compounds were identified and are shown in Figs. 4 and 5, respectively, and significant biomarker parameters were calculated and are shown in Table 2 based on their relative abundances in the representative mass chromatograms.

The mass chromatograms of m/z 191 showed the relative abundance of $C_{19} \sim C_{25}$ tricyclic terpanes in the studied samples (Fig. 4). The tricyclic terpane compounds displayed a normal distribution in the relative abundance with a peak of C_{21} tricyclic terpane ($C_{21}TT$) in most samples. Higher amounts of C_{20} tricyclic terpane ($C_{20}TT$) relative to C_{21} tricyclic terpane ($C_{21}TT$) were also observed in some samples such as sample MN1-6 (Fig. 4B). Moreover, the biomarkers were quantitatively investigated to calculate the content percentage among the $C_{19} \sim C_{23}$ tricyclic terpane compounds. The sum percentages of $C_{19}TT$ and $C_{20}TT$ were measured in a range of 27.93% ~ 49.96%, in which the highest percentage was found in the sample MN1-2 of the Kezilenuer Formation. The C_{23} tricyclic terpane ($C_{23}TT$) compound was typically detected in a low abundance in all samples, varying from 16.48 to 33.87%. The $C_{21}TT$ compounds were detected in relative contents of 31.87% ~ 40.52% in the Jurassic samples. Interestingly, most samples from the Ahe Formation displayed a predominance of $C_{21}TT$ components. However, the majority of the samples from the Kezilenuer Formation had a higher abundance of $C_{19}TT$ and $C_{20}TT$ rather than $C_{21}TT$.

The distributions of C_{27} to C_{29} regular steranes were identified along with remarkable differences in the representative reservoir samples, as shown in the m/z 217 mass chromatograms of the saturated hydrocarbon sections. There were three types of regular sterane distributions according to their relative abundances. The predominance of C_{27} regular sterane ($C_{27}ST$) was present in the extracted hydrocarbon from the Kezilenuer Formation, forming an "L" shape (Fig. 5A,B). A few samples were dominated by C_{29} regular steranes ($C_{29}ST$), showing an inverse "L" type in the sediments from the Yangxia Formation (Fig. 5C,D). Additionally, there was a very similar abundance in $C_{27}ST$ and $C_{29}ST$, characterized by a "V" pattern in the samples from the Ahe Formation (Fig. 5E,F,G,H). A relatively
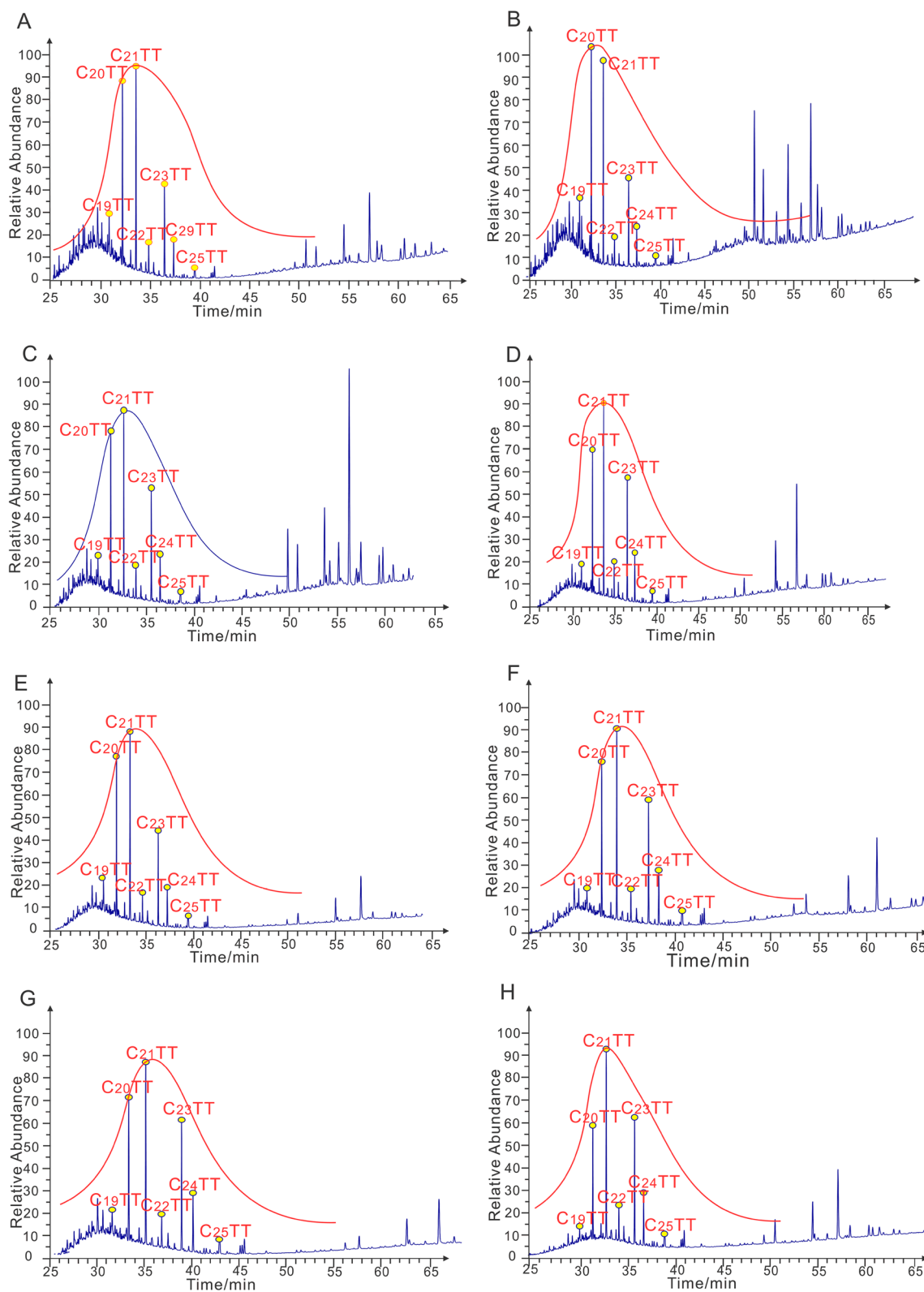
Fig. 4 Mass chromatograms of saturated hydrocarbon fractions showing distributions of tricyclic terpanes (*m/z* 191) in the representative samples from Jurassic reservoir of Well MN1. **A**: 417.2 m, J_2kz, gray medium sandstone; **B**: 607.5 m, J_2kz, gray coarse sand conglomerate; **C**: 777.8 m, J_1y, gray coarse sand conglomerate; **D**: 781.9 m, J_1y, gray coarse sandstone; **E**: 951.7 m, J_1a, gray medium sandstone; **F**: 963.9 m, J_1a, gray medium coarse sandstone; **G**: 1024.8 m, J_1a, gray coarse sandstone; **H**: 1084.5 m, J_1a, gray conglomerate. *TT* tricyclic terpane
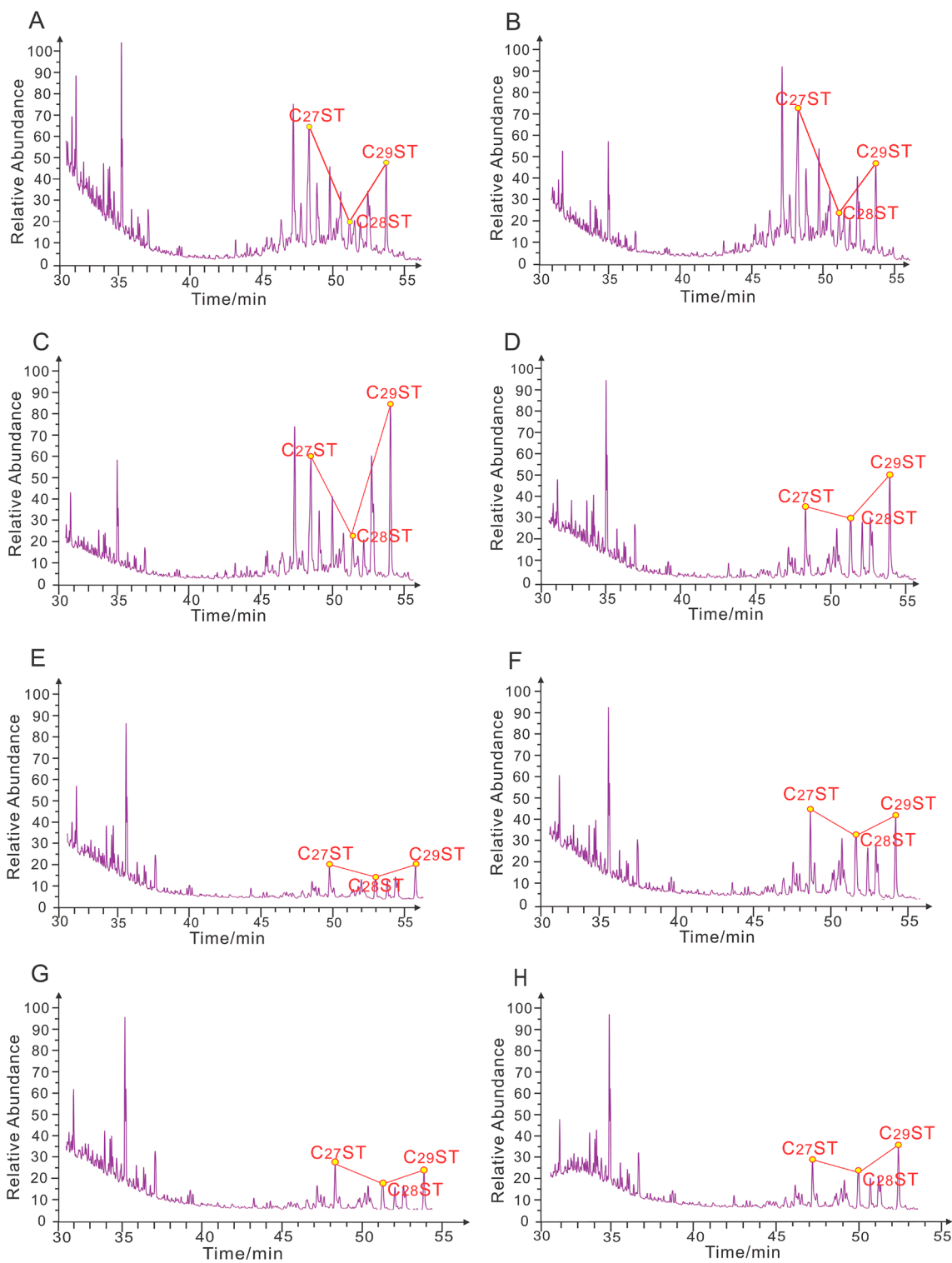
Fig. 5 Mass chromatograms of the saturated hydrocarbon fractions showing distributions of regular steranes (m/z 217) in the representative samples from the Jurassic reservoir of Well MN1. **A**: 417.2 m, J_2kz, gray medium sandstone; **B**: 607.5 m, J_2kz, gray coarse sand conglomerate; **C**: 777.8 m, J_1y, gray coarse sand conglomerate; **D**: 781.9 m, J_1y, gray coarse sandstone; **E**: 951.7 m, J_1a, gray medium sandstone; **F**: 963.9 m, J_1a, gray medium-coarse sandstone; **G**: 1024.8 m, J_1a, gray coarse sandstone; **H**: 1084.5 m, J_1a, gray conglomerate. *ST* regular sterane

Table 2 Biomarker parameters in the saturated hydrocarbon fractions for studied samples

Sample No	Tricyclic terpanes			Regular steranes			
	%C19+C20TT	%C21TT	%C23TT	%C27ST	%C28ST	%C29ST	C27/C29ST
MN1-1	44.80	36.30	18.90	64.48	5.34	30.19	2.14
MN1-2	49.96	31.87	18.16	68.00	9.71	22.28	3.05
MN1-3	45.39	35.58	19.03	35.75	15.55	48.70	0.73
MN1-4	36.99	36.36	26.65	27.86	28.66	43.47	0.64
MN1-5	32.54	33.59	33.87	25.86	29.52	44.61	0.58
MN1-6	49.51	34.00	16.48	62.47	11.42	26.12	2.39
MN1-7	39.57	35.93	24.50	43.00	12.19	44.81	0.96
MN1-8	31.62	36.29	32.09	26.41	29.57	44.02	0.60
MN1-9	34.91	37.62	27.47	29.12	28.25	42.63	0.68
MN1-10	41.66	36.78	21.56	37.74	26.40	35.87	1.05
MN1-12	36.51	36.39	27.09	30.09	35.91	33.99	0.89
MN1-13	36.67	37.17	26.16	37.72	28.76	33.52	1.13
MN1-15	34.63	36.53	28.84	37.24	28.66	34.11	1.09
MN1-16	33.72	35.11	31.16	29.52	19.30	51.18	0.58
MN1-18	34.34	36.19	29.47	32.88	26.89	40.24	0.82
MN1-19	35.99	36.82	27.20	38.66	23.02	38.31	1.01
MN1-20	27.93	39.07	33.01	26.53	27.39	46.08	0.58
MN1-21	28.73	40.52	30.75	32.66	29.45	37.89	0.86

TT tricyclic terpane; *ST* regular sterane

higher abundance of C_{27} regular steranes was detected in most samples, and its percentage content was in the range of 26.41% ~ 68.00% (averaging 38.11%). $C_{29}ST$ was the second most abundant component in the samples, showing a relative abundance of 22.28% ~ 51.18% (averaging 38.78%). The $C_{27}/C_{29}ST$ ratios were in the range of 0.58 ~ 3.05, reflecting a significant variation in the Jurassic samples. The lowest value of $C_{27}/C_{29}ST$ was 0.58, which was from the MN1-20 sample.

Petrographic characteristics of the fluid inclusions

Minor amounts of hydrocarbon-bearing fluid inclusions and coexisting aqueous inclusions were observed in the selected samples throughout the Jurassic reservoir. In particular, fluid inclusions were relatively widely trapped by quartz in the Ahe Formation. Hydrocarbon inclusions were distinguished from aqueous inclusions according to their fluorescent properties. In addition, the petrographic characteristics of the petroleum inclusions were significantly helpful to classify them into different categories. In this study, these inclusions were classified into two types of hydrocarbon inclusions and associated aqueous inclusions within the Jurassic reservoir according to petrographic observations. They are shown in Fig. 5 and described as follows.

i. Some hydrocarbon inclusions fluoresced yellow and were accompanied with colorless aqueous inclusions under UV observation. However, these oil inclusions appeared colorless in transmitted light. The inclusions were distributed in a cluster or scattered off the host grains (Fig. 6A,B,C), with a diameter of 6~10 μm in circle, elliptical, or irregular shapes. Obviously, the pure liquid-phase petroleum inclusions of yellow fluorescence color were developed in the quartz grain (Fig. 6A) or found along micro-fractures in line distributions (Fig. 6B). Few oil inclusions located in the quartz mineral surface were presented in the gas–liquid phase, but were dominated by the liquid phase (Fig. 6C). The oil inclusions also contained a colorless bubble under transmitted light, while the bubble had a dark color under ultraviolet light.

ii. Other hydrocarbon-bearing fluid inclusions showed blue-white fluorescence color under UV and were colorless in the transmitted light. Their amounts were lower than that of the yellow fluorescent oil inclusions. Generally, the inclusions showed a pure liquid phase with a small diameter of 4~8 μm and occurred in elliptical or irregular shapes. Under the microscope, these inclusions were gathered in the corrosion hole of the detrital grains (Fig. 6D) or at the contact of the detrital grains (Fig. 6E). Similar to the oil inclusions with yellow fluorescence, the blue-white fluorescent petroleum inclusions were also found in a line distribution along the micro-fractures (Fig. 6F).

Fig. 6 Photomicrographs of hydrocarbon inclusions under transmitted and ultraviolet light. **A**: 1154.6 m, J$_1$a, medium sandstone, pure colorless liquid-phase oil inclusions under transmitted light showing yellow fluorescence under ultraviolet light; **B** and **C**: 1032.2 m, J$_1$a, coarse sand conglomerate, colorless oil inclusions under transmitted light showing yellow fluorescence under ultraviolet light, present pure liquid and gas–liquid phase, respectively; **D**: 1032.2 m, J$_1$a, coarse sand conglomerate, pure colorless liquid-phase oil inclusions under transmitted light showing blue-white fluorescence under ultraviolet light; **E**: 1034.8 m, J$_1$a, coarse sandstone, colorless oil inclusions under transmitted light showing blue-white fluorescence under ultraviolet light; **F**: 1081.3 m, J$_1$a, coarse sand conglomerate, pure colorless liquid-phase oil inclusions under transmitted light showing blue-white fluorescence under ultraviolet light
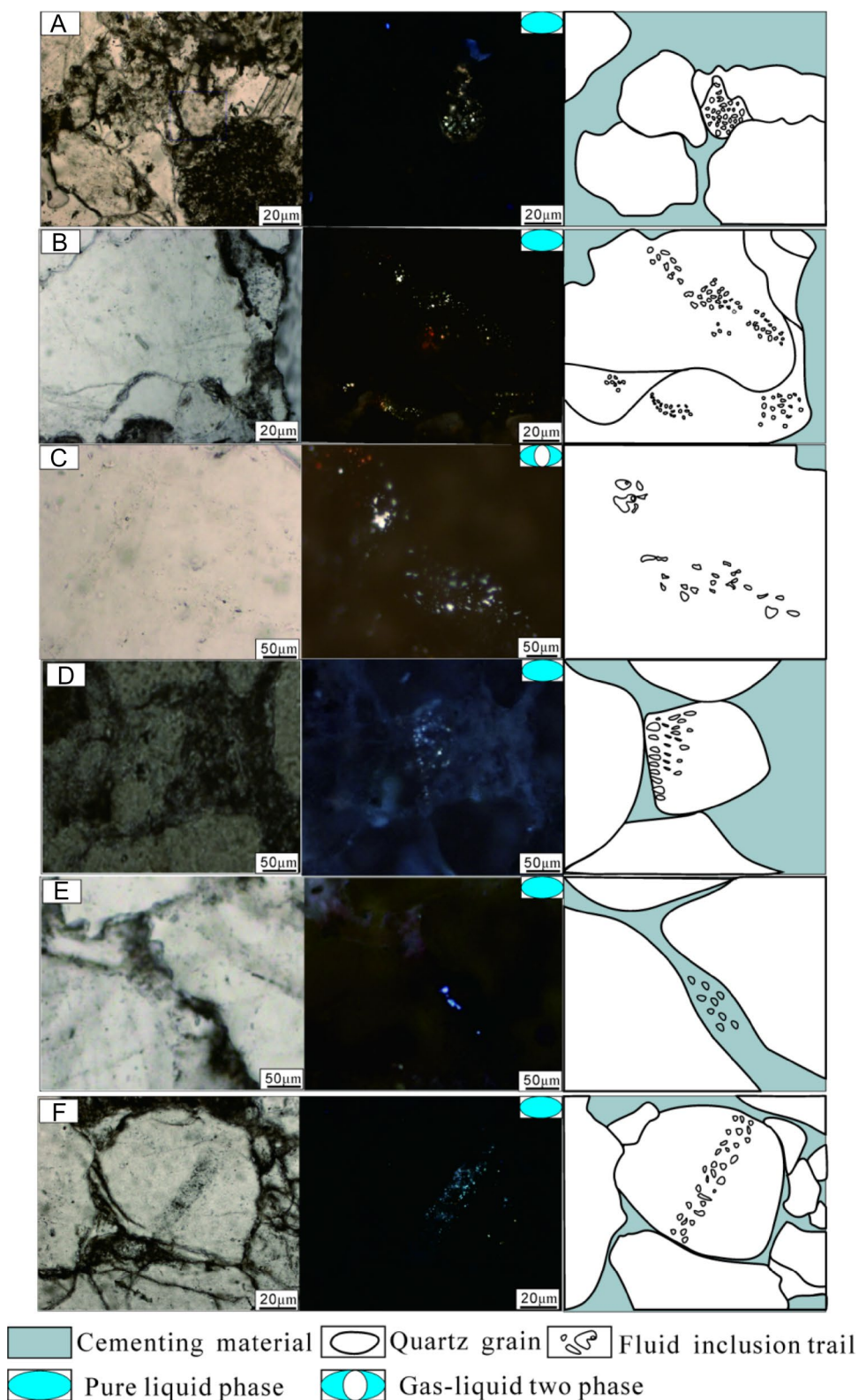
Fig. 7 Burial history of well MN 1 in the eastern Kuqa Depression
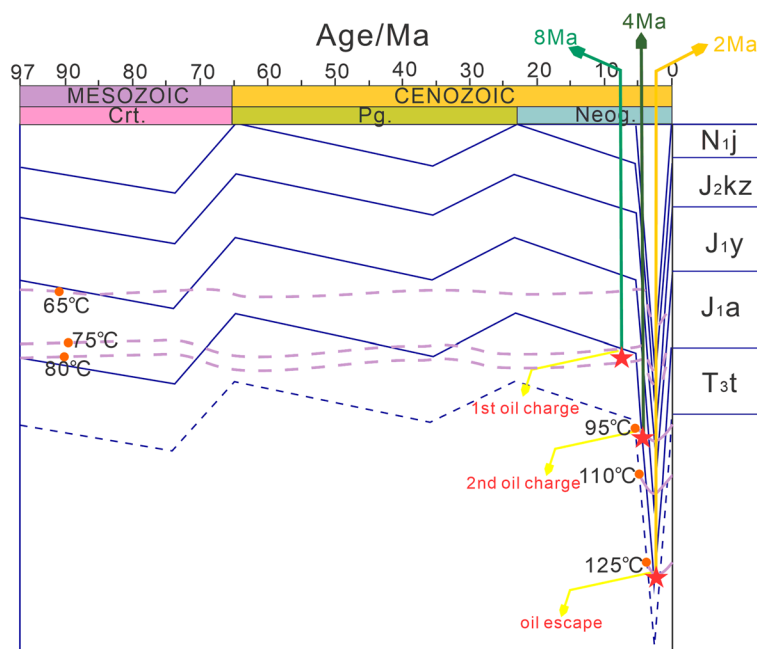
Homogenization temperature and charging age of the fluid inclusions

Due to the different shrinkage rates of the bubbles inside the inclusions, there was a significant difference in the mean temperature of the hydrocarbon inclusions and the accompanying brine inclusions with a difference of 20~40 ℃ (Shi et al. 1987). The homogenization temperature (Th) measurements of the variable inclusion assemblage played a vital role in the analysis of the hydrocarbon charging phases. The burial history of the reservoirs in the study area was reconstructed using the PetroMod 1D simulation software (Fig. 7). The time of hydrocarbon expulsion was determined based on the homogenization temperature values of the different kinds of aqueous inclusions, which was related to the stability of the brine inclusion's properties during the burial process (Bourdet et al. 2008).

The geothermal gradient of the Kuqa Depression was relatively low, being estimated to be in the range of 2.9~3.2 °C/100 m during the Mesozoic, around 2.9 °C/100 m during the Paleogene and Neogene, and around 2.5 °C/100 m at present (Wang et al. 2000). The Th values of the coeval aqueous inclusions associated with the yellow fluorescent hydrocarbon inclusions were calculated to be in the range of 80~95 °C, which corresponded to the burial age of 6~4 Ma. Additionally, the aqueous fluid inclusions associated with the blue-white fluorescent hydrocarbon inclusions had Th values of 105~120 °C, which was consistent with the burial age of 4~2 Ma.

QGF and QGF-E responses

The fluorescence spectroscopy technique can accurately identify the compositions and properties of hydrocarbons that are adsorbed on reservoir surfaces or in particles to detect paleo-oil or residual-oil deposits (Liu et al. 2007). The spectral parameters were expressed by the QGF index, the QGF-E intensity, and the maximum wavelength (λ max). The QGF index values had an average spectral intensity between 375 and 475 nm, and were normalized to a spectral intensity at 300 nm. The QGF-E intensities were described as the maximum spectral intensities normalized to 1 g of quartz sand in 20 ml of DCM solvent. The results of previous research (Liu and Eadington 2005) indicated that paleo-oil layers usually exhibited strong QGF index values greater than 4, whereas the values of water layers were usually below 4. In addition, residual-oil layers usually had strong QGF-E intensities greater than 40 photometer counts (pc), whereas the values below 20 pc were considered to be water layers.

The results of the QGF and QGF-E analyses at the depth interval between 417.2 m and 1154.6 m in the Jurassic reservoir are given in Fig. 8 and Table 3. The QGF index and QGF-E intensity parameters were measured on the rock samples to determine the development of the paleo and current reservoir. The QGF index values ranged from 0.34 to 6.65, with the maximum value at a depth of 1029 m in the Ahe Formation, which showed an increasing trend as the burial depth decreased. The deepest sample (MN1-24) had the lowest QGF index value of 0.34. It should be noted that the locations below 1084.5 m had QGF index values in the range of 0.34~0.38, while all the samples above had values higher than 4.00. This indicated that the depth of
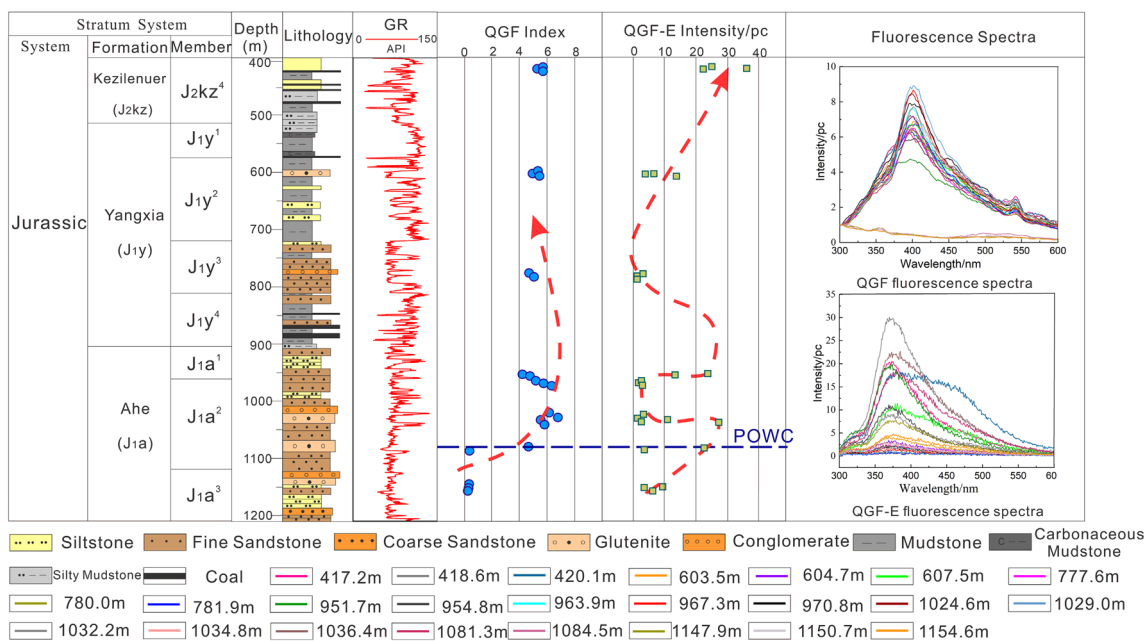
Fig. 8 Stratigraphic profiles of the quantitative grain fluorescence (QGF) index, QGF on extract (QGF-E) intensity, and the fluorescence spectra of well MN 1 in the eastern Kuqa Depression. The QGF index is the average spectral intensity between 375 and 475 nm normalized to the spectral intensity at 300 nm. The QGF-E intensity is the maximum spectral intensity of a QGF-E spectrum normalized to weight and volume. POWC means paleo oil–water contact

1084.5 m could be considered to be a paleo-oil–water contact (POWC). Additionally, the QGF fluorescence spectra of all the samples were obtained. The four deepest samples displayed weak spectrum responses. The other samples presented a unimodal distribution with a distinct peak around 400 nm in the QGF fluorescence emission of the fluorescence spectra, which was coincident with the features of medium crude oils. The QGF-E intensity values were lower than 40.00 photometer counts in all samples. The maximum value of 36.15 photometer counts was obtained from the sample MN1-2. Unlike the variation trend of the QGF index values, the QGF-E intensity presented a complex change distribution as shown in Fig. 8. On the whole, it displayed an increasing upward trend with decreasing burial depths in the Jurassic strata interval. The QGF-E fluorescence spectra were characteristic of a similar regular pattern in all current samples. Furthermore, the λ max values ranged from 360 to 390 nm, which were lower than that of the QGF fluorescence spectra. This indicated that the residual oil in the reservoir showed the typical features of condensate oil.

Discussion

Identification of source rocks for oil generation

The correlation between oil and source rocks is key to identifying the organic matter types for hydrocarbon generation
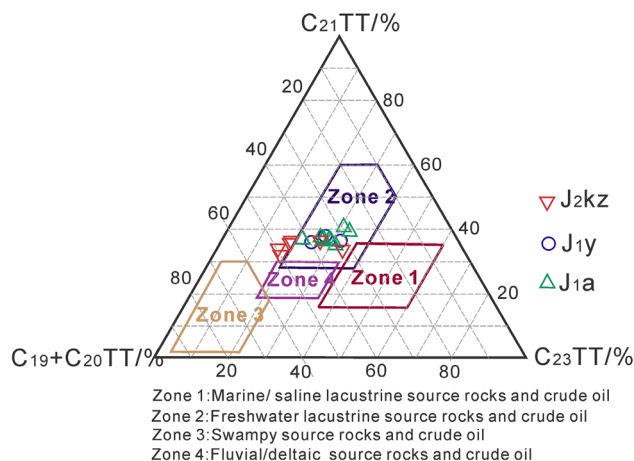
and investigating the geological problems of hydrocarbon accumulation (Peters et al. 2005a, b). Qualitative and quantitative analyses of biomarkers in source rocks or crude oil are performed through gas chromatography–mass spectrometry experiment to reveal the type of parent material and the sedimentary environment during deposition of the organic matter (Alberdi et al. 2001; Guo et al. 2015; Tang et al. 2019). Furthermore, Liu et al (2019) showed that the measured maturity of Jurassic oil was approximately 1.0%, which indicated that the biomarkers in the extracted oil samples were helpful for identifying the geologic features of the organic matter.

Tricyclic terpanes are regarded as effective indicators of organic matter types resulting from different relative amounts of diverse organic matter sources (Ekweozor 1981; Bao et al. 1999). It has been proposed that compounds with carbon numbers less than 21 in the tricyclic terpane series are derived from higher plants (Ekweozor 1981). Moreover, the predominance of the $C_{19}TT$ compounds is generally accepted as the typical feature of coal-formed oil (Bao et al. 1999; Tao et al. 2015). In the Kuqa Depression, previous studies have demonstrated that the tricyclic terpanes of coal-measure source rocks show a stepped distribution pattern with a prominent peak of $C_{19}TT$, displaying a decreasing trend in the relative abundance of tricyclic terpanes with increasing carbon numbers (Liu et al. 2018; Li et al. 2019). Higher abundances of $C_{21}TT$ or $C_{23}TT$ in the tricyclic terpane series reflect the contributions of aquatic organisms,

Table 3 Quantitative grain fluorescence (QGF) and QGF on extract (QGF-E) parameters of the studied samples

Sample No	QGF			QGF-E	
	Index	Intensity/pc	λ max/nm	Intensity/pc	λ max/nm
MN1-1	5.60	0.69	395.56	24.60	373.00
MN1-2	5.30	0.69	396.68	36.15	370.00
MN1-3	5.68	0.65	399.41	22.32	379.00
MN1-4	5.34	0.98	401.02	5.76	375.00
MN1-5	5.07	1.16	403.16	4.12	369.00
MN1-6	5.41	1.15	399.28	13.76	381.00
MN1-7	4.81	1.36	399.92	2.76	365.00
MN1-8	4.82	1.42	400.92	1.13	386.00
MN1-9	5.08	1.54	399.43	1.05	372.00
MN1-10	4.23	0.76	396.28	23.86	374.00
MN1-11	4.78	0.85	397.05	13.32	369.00
MN1-12	5.20	1.69	400.30	2.68	377.00
MN1-13	5.89	1.77	401.29	1.71	384.00
MN1-14	6.23	1.10	399.17	2.29	366.00
MN1-15	6.10	1.81	400.29	2.93	365.00
MN1-16	6.65	1.43	403.38	1.43	372.00
MN1-17	5.69	1.39	401.66	11.01	364.00
MN1-18	5.73	1.19	399.93	2.26	373.00
MN1-19	5.74	1.20	399.54	27.25	385.00
MN1-20	4.61	1.76	402.53	22.58	380.00
MN1-21	0.38	0.27	306.19	3.64	375.00
MN1-22	0.37	0.19	312.05	9.36	379.00
MN1-23	0.37	0.22	309.44	3.60	373.00
MN1-24	0.34	0.18	303.81	5.21	369.00

Fig. 9 Relative abundances of tricyclic terpane biomarker parameters for determining depositional environments

which occur in the Triassic source rocks with a normal distribution in the corresponding mass chromatograms (Tang et al. 2019). This was to say that the Jurassic hydrocarbon was mainly originated from algal organic matter, consistent with a normal distribution in the relative abundances with a peak at $C_{20}TT$ or $C_{21}TT$ in the tricyclic terpane series. Additionally, regular steranes also are remarkable parameters for determining the biological sources of oil and source rocks (Peters and Moldowan 1993). The relative contents of C_{29} and C_{27} regular steranes are often used as evidence to distinguish distinct types of organic matter, where higher contents of C_{29} regular steranes indicate a larger contribution of higher plants (Peters et al. 2005b). Coal-derived oil is present as inverse "L" patterns in the relative abundance of $C_{27} \sim C_{29}$ regular steranes, while organic matter mainly from aquatic organisms shows an "L" shape pattern (Zhao et al. 1998). Almost all the samples in this study had abundant $C_{27}ST$ compounds and presented an "L" shape in the representative mass chromatograms, indicating a much higher contribution from aquatic organisms. Some samples displayed a similar abundance of $C_{27}ST$ and $C_{29}ST$, and

C_{27} ST /C_{29} ST ratios of approximately 1.0, supporting an algal input into the source rocks. Nevertheless, a few samples had higher contents of $C_{29}ST$ in the regular steranes with an inverse " L"-shaped distribution pattern, confirming that some terrestrial plants also contributed to hydrocarbon generation. The tricyclic terpane distributions in the studied samples also reflected the depositional environment of the organic matter. High concentrations of C_{21} tricyclic terpanes were characteristic of sediments deposited in freshwater lacustrine environments, while abundant C_{23} tricyclic terpanes were strongly related to saline lacustrine depositional environments. C_{19} and C_{20} tricyclic terpanes were recorded in high abundance under swampy environments (Xiao et al. 2019). Taking the quantitative analysis of the relative abundances of $C_{19}+C_{20}TT$, $C_{21}TT$, and $C_{23}TT$ compounds and placing them into the sedimentary environments chart established by Xiao et al (2019) (Fig. 9), it was found that most of the parameter points exhibited a relatively clustered distribution, and were concentrated in the freshwater lacustrine environment zone.

Based on this source rock-oil correlation from the biomarker information, it was inferred that the crude oil of the Ahe Formation was mainly generated from the lower Triassic lacustrine mudstone, which was deposited in a freshwater environment. The petroleum in the Kezilenuer and Yangxia formations was mainly generated from the Triassic lacustrine mudstone, with some contribution from Jurassic coal measure source rocks. This conclusion was similar to that of the source rocks of the Jurassic hydrocarbons in the Dibei area, indicating that the Jurassic strata in the eastern Kuqa Depression had the potential to have formed oil and gas reservoir (Li et al. 2019).

## Characteristics of the hydrocarbon charging phases

Hydrocarbon charging characteristics are determined by the matching of tectonic activity periods and hydrocarbon generation and expulsion history (Zeng 2004). The strong lateral compression in the Himalayan orogeny led to the uplift of Mt. Tianshan and the subsidence of the Kuqa Depression, thereby influencing the thermal evolution of the source rocks in the Mesozoic strata (Zhao and Dai 2002). The sediments underwent slow subsidence in the Mesozoic and uplift in the Late Cretaceous, resulting in a low maturity of the Triassic and Jurassic source rocks before the Late Tertiary (Du et al. 2006). Since the Neogene, the rapid burial of Mesozoic strata accelerated the thermal evolution of organic matter, causing the Triassic source rocks to reach the peak of their oil generation capacity in the early Neogene. However, the Jurassic source rocks reached their peak oil generation capacity in the Neogene when the Triassic source rocks quickly entered the generation stage of wet gas and dry gas (Wang et al. 1999; Zhao and Lu 2003).

Fluid inclusion analyses have been widely used in petroleum geology research to provide important insights into the processes and timing of hydrocarbon migration in structurally complex basins (Goldstein 2001). The fluorescence properties of hydrocarbon inclusions are related to the thermal evolution of oil. The hydrocarbon shows more stable and strongly polar fluorescent components with the increasing maturity (Stasiuk and Snowdon 1997; George et al. 2001). The fluorescence colors vary from brown to blue when the hydrocarbon compositions change from heavy oil to condensate oil, respectively (Hagemann and Hollerbach 1986; George et al. 2001). Moreover, the maximum fluorescence emission values in the spectral measurements can be used as an indicator of thermal maturity (Liu et al. 2016). Generally, the higher of crude oil density, the more content of heavy oil, and the higher λ max values is present.

Consequently, two episodes of hydrocarbon charge were identified based on the detailed study of fluid-inclusion petrography, microthermometry, and fluorescence spectroscopy characteristics. The spatio-temporal distribution of the hydrocarbon charging activity and the thermal evolution of the source rocks were analyzed based on the simulated thermal evolution history. It was suggested that the first charging stage was characteristic of mature oil during the late Miocene to early Pliocene (circa 6 ~ 4 Ma), resulting in higher λ max values and yellow fluorescence colors. At that time, the Triassic source rocks entered into the oil-generating window, while the Ro of the Jurassic coal-measure source rocks was distributed in the immature stage (Fig. 10). The oil inclusions with the fluorescence colors of blue-white and the coexisting aqueous inclusions recorded the second period of oil charging, which was corresponded to the Pliocene (4 ~ 2 Ma). Both the presence of the smaller λ max values in the QGF-E fluorescence spectra and the blue-white fluorescence of the oil inclusions indicated that the oil was dominated by a light composition in the form of condensate oil. During this period, Jurassic source rocks entered the oil window and produced mature oil, and the Ro of the Triassic source rocks could reach 0.9%. This was to say that the light oil in the Jurassic reservoir was sourced by Triassic mudstones rather than Jurassic coal seams. Previous studies on the tectonic

Fig. 10 The thermal evolution of well MN 1 in the eastern Kuqa Depression
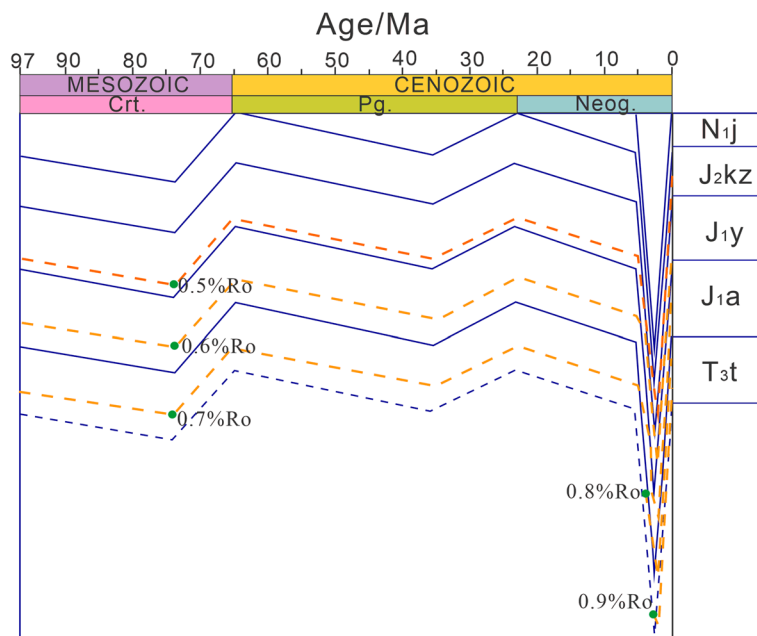
evolution of the study area (Chai et al. 2020) showed that the main thrust fault in the area was well developed since the Miocene and the fault have provided a dominant vertical migration conduit for oil. The oil generated from the Triassic source rocks could migrate into the Jurassic reservoir along the fault. In addition, fractures were formed by the tectonic activity and they supported the lateral oil migration channels. Therefore, small amounts of mature oil from Jurassic coal-measure source rocks were expelled into the reservoirs with high-quality physical properties. In contrast to the three stages of oil and gas charging in the Jurassic reservoir of the Dibei area (Li et al. 2019), there were only two episodes of oil charging in the Jurassic strata, which was due to the shallow burial of the Mesozoic strata and the medium thermal maturity of the source rocks, making it difficult to generate natural gas.

Process and mechanism of hydrocarbon accumulation

Favorable fault structure development, large-scale hydrocarbon charging, and trap formation are necessary conditions for hydrocarbon accumulation. The Kuqa Depression has experienced multi-stage tectonic movements, marked by the Cretaceous Yanshan movement and the Tertiary Himalayan movement, with the former serving as the key period to form faults and structures in the depression, characterized by a series of northward thrust faults that formed under the large horizontal extrusion force of the Tianshan Mountains. Moreover, a series of east–west linear anticlines were present in the Kuqa Depression and these were influenced by the rising Tianshan Mountains and the movement of faults during the late Himalayan movement (Qin et al. 2002). The Yiqikelike structural belt in the eastern Kuqa Depression had folds and thrust deformations, and numerous thrust faults and fault anticlines have formed in the Mesozoic strata (Shang et al. 2012). In particular, intense tectonic deformation was present in the Tugerming area and these were controlled by palaeo-uplifts in the early; furthermore, the strata has experienced late erosion (Zhang et al. 2019). The Mesozoic-Cenozoic tectonic evolution and hydrocarbon accumulation mechanism in the eastern Kuqa Depression were seriously affected by the Himalayan orogeny, which provided the main impetus for structural movement (Charreau et al. 2006). The intensity of the structural activity was relatively weak from the Neogene to the Miocene and the strong compression of the strata due to the active Himalayan orogeny played an essential role in the hydrocarbon charging during the Pleistocene to Quaternary; further, the structural features were finalized during the deposition of the Kuqa Formation in response to the peak of the Himalayan movement (Zhang et al. 2019). Multi-channel seismic data throughout MN1 have been interpreted to reveal the

characteristics of the Mesozoic tectonic deformation in the Tugerming area (Fig. 2D). The reservoir properties and the hydrocarbon generation, migration, accumulation, adjustment, and preservation history were primarily controlled by the tectonic activity of the southern Tianshan Mountains because tectonic compression produced rapid sedimentation and thrust-fault reactivation (Jia and Li 2008).

The Triassic mudstone and Jurassic coal-measure source rocks could supply sufficient organic matter for hydrocarbon generation, and regional mudstone rocks in the Neogene Jidike Formation acted as effective cap rocks in the Kuqa Depression (Jia 1999). Multiple sets of sandstone reservoir were developed in the Jurassic strata, and the Lower Jurassic reservoir was regarded as the preferred reservoir space for hydrocarbon migration, which were controlled by dissolution and primary intergranular pores with higher porosity and permeability (Li et al. 2018). The peak period of oil and gas generation and the formation period of traps in the Kuqa Depression were in the late Kuche period, and, thus, the hydrocarbon accumulation must have occurred recently, which was conducive to the formation of large- and medium-sized gas fields (Zhao and Lu 2003). There were two sets of hydrocarbon accumulation models developed for the Jurassic strata: (a) the lower-generation and upper-storage model and (b) the self-generated and self-stored model (Fig. 11).

During the Middle and Late Miocene (6 ~ 4 Ma), the Triassic source rocks entered the low-mature stage and a small number of oil inclusions in yellow fluorescence color became trapped in the sandstone. However, the organic matter in the Jurassic strata was immature because of the shallow burial depth. At that stage, the early thrust fault formed a low amplitude anticlinal structure driven by the compression from the South Tianshan Mountains. At the same time, faults were active and provided channels for hydrocarbon migration (Shang et al. 2012). The mature oil mainly generated from the Huangshanjie Formation was expelled into the Ahe Formation along faults under the force of buoyancy to form paleo-oil reservoirs. Consequently, this hydrocarbon accumulation mechanism was regarded as lower-generation and upper-storage model.

During the Pliocene Epoch (4 ~ 2 Ma), as the burial depth quickly increased, the source rocks in the Jurassic and Triassic strata experienced rapid thermal maturation due to the uplift of Mt. Tianshan. Consequently, the vitrinite reflectance of the Jurassic source rock (estimated at 0.5~0.7%) showed that the source rocks generated mature oil that migrated and was stored in the Kezilenuer and Yangxia formations. This hydrocarbon accumulation mechanism was of the self-generated and self-stored model. The Triassic organic matter generated condensate oil that migrated into Jurassic reservoir. At the same time, the amplitude of the structural uplift became larger under the intense compression caused by tectonic activities of South Tianshan. The

Fig. 11 Hydrocarbon accumulation process in the Jurassic reservoir of the eastern Kuqa Depression. **A**: During 6~4 Ma, mature oil was generated and expelled to charge the Jurassic reservoir; **B**: During 4~2 Ma, the light oil was expelled into the Jurassic reservoir; **C**: Since the Quaternary, most of the oil escaped to the surface, with a small amount remaining in the reservoir
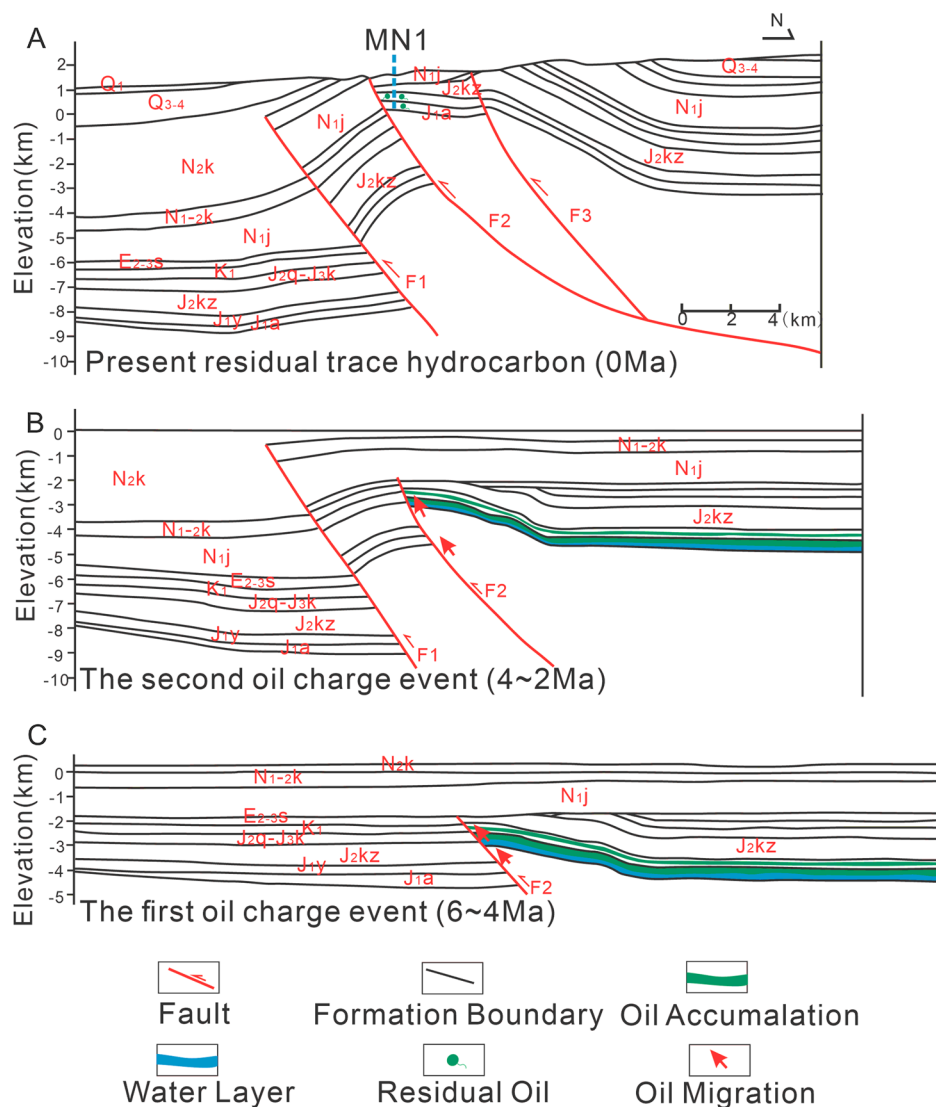
light oil effectively accumulated in the trapping structure and was associated with the blue-white fluorescence color of the oil inclusions.

The period since the Quaternary was the time of structural finalization that corresponded with the late Himalayan orogeny movements. The strong tectonic activity of the Himalayan orogeny during the late evolutionary period provided the main force for structural movement (Charreau et al. 2006). The anticline's core was subjected to intense uplifting and denudation. The fault cut through the upper mudstone cap rocks to the surface, and the strata in the structural high were uplifted and denuded, and thus the old oil reservoirs suffered from severe destruction and abundant oil was lost to the surface. Similarly, the Dibei gas field has experienced strong tectonic compression associated with intense thrust-fault reactivation (Pang et al. 2019); however, several thick mudstones and gypsum mantles cover the natural gas reservoirs and the conservation of the natural gas was superior in the Dibei area (Li et al. 2015).

Summary and conclusions

(1) The petroleum in the Jurassic reservoir was mainly derived from Triassic mudstones deposited in freshwater lakes, with some contribution from Jurassic coal measure source rocks.

(2) The integrated analysis of fluid inclusions composed of petrography observations, microthermometry measurements, and fluorescence spectroscopy showed that there were two periods of oil charging in the Jurassic reservoir (corresponding to 6~4 Ma and 4~2 Ma).

(3) We integrated the fluid inclusions and biomarker compounds experiments to systematically discuss the mechanism of hydrocarbon accumulation in the Jurassic res-

ervoir. There were two accumulation models including the lower-generation and upper-storage model and the self-generated and self-stored model. It indicated that the study area had great oil and gas exploration potential.

(4) Tectonic activities significantly controlled the accumulation mechanism and the preservation of the oil reservoir. A large amount of stored hydrocarbon was escaped to the surface due to poor preservation conditions resulting from the strong denudation of the shallow-buried strata.

Declarations

Conflict of interest The author(s) declared no potential conflicts of interest with respect to the research, authorship, and/or publication of this article.

References

Alberdi M, Moldowan JM, Peters KE, Dahi E (2001) Stereoselective biodegradation of tricyclic terpanes in heavy oils from the Bolivar coastal fields. Venezuela Org Geochem 32:181–191

Anees A, Zhang H, Ashraf U, Wang R, Liu K, Abbas A, Ullah Z, Zhang X, Duan L, Liu F, Zhang Y, Tan S, Shi W (2022) Sedimentary facies controls for reservoir quality prediction of lower shihezi member-1 of the Hangjinqi area. Ordos Basin Miner 12:126

Anees A, Shi W, Ashraf U, Xu Q (2019) Channel identification using 3D seismic attributes and well logging in lower Shihezi Formation of Hangjinqi area, northern Ordos Basin, China. J Appl Geophys 163:139–150

Bao JP, Ma AL, Huang GH, Li XQ, Zhong NN (1999) The Origin and geochemical characteristics of crude oils from Santanghu basin. Petrol Explor Dev 26:25–29

Bourdet J, Pironon J, Levresse G, Tritlla J (2008) Petroleum type determination through homogenization temperature and vapour volume fraction measurements in fluid inclusions. Geofluids 8:46–59

Burnham AK, Sweeney JJ (1989) A chemical kinetic model of vitrinite maturation and reflectance. Geochimi Cosmochim Acta 53:2649–2657

Burruss RC, Cercone KR, Harris PM (1983) Fluid inclusion petrography and tectonic-burial history of Al Ali No. 2 well: evidence for the timing of diagenesis and oil migration, northern Oman foredeep. Geol 11:567–570

Chai S, Li C, Lu X, Zhuo Q, Gong Y (2020) Geometry and kinematics of tugerming structural belt in the east of Kuqa Depression, Tarim Basin. Petrol Res 6:333–350

Charreau J, Gilder S, Chen Y, Dominguez S, Avouac JP, Sen S, Jolivet M, Li YG, Wang WM (2006) Magnetostratigraphy of the yaha section, Tarim basin (China): 11 Ma acceleration in erosion and uplift of the TianShan Mountains. Geol 34:181–184

Chen JP, Cha M, Zhu Y (2000) Application of organic inclusion in oil-gas migration. Geol Sci Technol Inf 1:61–64

Dai JX, Ni YY, Wu XQ (2012) Tight gas in China and its significance in exploration and exploitation. Pet Explor Dev 39:277–284

Du ZL, Wang FY, Zhang SC, Zhang BM, Liang DG (2006) Gas generation history of Mesozoic hydrocarbon kitchen in Kuqa Depression, Tarim Basin. Geochimica 4:419–431

Ekweozor CM (1981) Tricyclic terpanes in the Athabasca oil sands: their geochemistry. Adv Org Geochem 6:746–766

George SC, Ruble TE, Dutkiewicz A, Eadington PJ (2001) Assessing the maturity of oil trapped in fluid inclusions using molecular geochemistry data and visually-determined fluorescence colours. Appl Geochem 16:451–473

Goldstein RH (2001) Fluid inclusions in sedimentary and diagenetic systems. Lithos 55:159–193

Guo S, Lyu X, Zhang Y (2018) Relationship between tight sandstone reservoir formation and hydrocarbon charging: a case study of a Jurassic reservoir in the eastern Kuqa Depression, Tarim Basin, NW China. J Nat Gas Sci Eng 52:304–316

Guo PF, He S, Zhu SK, Chai DR, Yin SY (2015) Application of tricyclic terpanes in biodegraded oil-source correlation in Biyang Sag. Pet Geol Exp 37:80–87

Guo XW, Liu KY, Jia CZ, Song Y, Zhao MJ, Lu XS (2016a) Effects of early petroleum charge and overpressure on reservoir porosity preservation in the giant Kela-2 gas field, Kuqa depression, Tarim Basin, northwest China. AAPG Bull 100:191–212

Guo XW, Liu KY, Jia CZ, Song Y, Zhao MJ, Zhuo QG, Lu XS (2016b) Fluid evolution in the Dabei gas field of the Kuqa Depression, Tarim Basin, NW China: implications for fault-related fluid flow. Mar Petrol Geol 78:1–16

Hagemann HW, Hollerbach A (1986) The fluorescence behaviour of crude oils with respect to their thermal maturation and degradation. Org Geochem 10:473–480

Haszeldine RS, Samson IM, Cornfort C (1984) Dating diagenesis in a petroleum basin: a new fluid inclusion method. Nat 307:354–357

He DF, Jia CZ, Li DS, Zhang CJ, Meng QR, Shi X (2005) Formation and evolution of polycyclic superimposed Tarim Basin. Oil Gas Geol 1:64–77

He DF, Li DS, He JY, Wu XZ (2013) Comparison in petroleum geology between Kuqa Depression and Southwest depression in Tarim Basin and its exploration significance. Acta Pet Sin 34:201–218

He GY, Lu HF, Li SX, Yang SF (2004) Features and dynamics for structure deformation of Yinan gas field in Kuqa Basin, Northwestern China. Acta Sci Nat Univ Pekin 40:247–252

Horsfield B, McLimans RK (1984) Geothermometry and geochemistry of aqueous and oil bearing fluid inclusions from Fatch field Dubai. Org Geochem 6:733–740

Jayanthi JL, Nandakumar V (2020) Fluid inclusion studies to determine the paleotemperature and hydrocarbon quality in petroliferous basins. J Pet Sci Eng 197:108082

Jia CZ (1999) Structural characteristics and oil/gas accumulative regularity in Tarim basin. Xinjiang Pet Geol 20:177–183

Jia CZ, Chen HL, Yang SF, Lu HF, Zhou YZ (2003) Late Cretaceous uplifting process and its geological response in Kuqa Depression. Acta Pet Sin 24:1–5

Jia CZ, Li QM (2008) Petroleum geology of Kela-2, the most productive gas field in China. Mar Petrol Geol 25:335–343

Ju Y, Sun XW, Liu LW, Xie YN, Wei HX (2014) Characteristics of Jurassic tight Sandstone gas reservoir in Dibei area of Kuqa Depression, Tarim Basin. Xinjiang Pet Geol 35:264–267

Li F, Jiang ZX, Li Z, Liu JL, Wang Y, Luo X (2016) Fluid inclusion characteristics and hydrocarbon charge history of Dibei gas reservoir in the Kuqa Depression. J Cent South Univ Technol Nat Sci 47:515–523

Li F, Jiang ZX, Li Z, Wang XH, Du ZM, Luo X, Xin SY (2015) Enriched mechanism of natural gas of lower Jurassic in Dibei area, Kuqa Depression. Earth Sci J China Univ Geosci 40:1538–1548

Li F, Jiang ZX, Pang XQ, Li F, Zhang BS (2013) Genetic types of the tight sandstone gas reservoirs in the Kuqa Depression, Tarim Basin, NW, China. J China Univ Geosci 38:156–164

Li GX, Yi SW, Lin SG, Gao Y, Li MP, Li DJ, Wang CY (2018) Reservoir characteristics and major factors influencing the reservoir quality of lower Jurassic in eastern Kuqa Depression, Tarim Basin. Nat Gas Geosci 29:1508–1517

Li J, Wang C, Li J, Ma W, Zhang HZ, Lu YH, Li DJ, Liu MC (2019) Source and exploration direction of tight oil and gas in the Dibei section of northern Kuqa depression. China Pet Explor 24:485–497

Liu HX, Wang D, Ji ZY, Zhao HQ (2018) Geochemical characteristics of source rocks from the Yinan 2 well in the eastern Kuche Depression. Resour Environ Eng 32:233–236

Liu KY, Bourdet J, Zhang BS, Zhang N, Lu XS, Liu SB, Pang H, Li Z, Guo XW (2013) Hydrocarbon charge history of the Tazhong Ordovician reservoirs, Tarim Basin as revealed from an integrated fluid inclusion study. Pet Explor Dev 40:171–180

Liu KY, Eadington P (2005) Quantitative fluorescence techniques for detecting residual oils and reconstructing hydrocarbon charge history. Org Geochem 36:1023–1036

Liu KY, Eadington P, Middleton H (2007) Applying quantitative fluorescence techniques to investigate petroleum charge history of sedimentary basins in Australia and Papuan New Guinea. J Pet Sci Eng 57:139–151

Liu KY, Lu XS, Gui LL, Fan JJ, Gong YJ, Li XL (2016) Quantitative fluorescence techniques and their applications in hydrocarbon accumulation studies. Earth Sci 41:373–384

Liu RH, Li J, Xiao ZY, Li J, Zhang HZ, Lu YH, Zhang BS, Ma W, Li DJ, Liu MC (2019) Geochemical characteristic and implication for gas and oil source correlation in the Tugerming area of the Kuqa Depression. Tarim Basin Nat Gas Geosci 30:574–581

Liu SB, Gu JY, (1997) Application of fluid inclusions to petroleum geological study and discussion. Oil Gas Geol, 8, 326-331, 342

Ma YJ, Xie HW, Cai ZZ, Zhang LJ, Gao GX (2003) The geology feature of dina2 as field, kuche depression. Nat Gas Geosci 5:371–374

Pang XQ, Peng JW, Jiang ZX, Yang HJ, Wang PW, Jiang FJ, Wang K (2019) Hydrocarbon accumulation processes and mechanisms in lower Jurassic tight sandstone reservoirs in the Kuqa subbasin,

Tarim Basin, northwest China: a case study of the Dibei tight gas field. AAPG Bull 4:769–796

Parnell J (2010) Potential of palaeofluid analysis for understanding oil charge history. Geofluids 10:73–82

Peters KE, Moldowan JM (1993) Interpreting molecular fossils in petroleum and ancient sediments. Prentice Hall, NJ, pp 1–236

Peters KE, Walters CC, Moldowan JM (2005) The biomarker guide: interpreting molecular fossils in petroleum and ancient sediments (second edition). Cambridge University Press, UK, pp 1–1155

Peters KE, Walters CC, Moldowan JM (2005b) The biomarker guide: volume 2 biomarkers and isotopes in petroleum systems and earth history. Cambridge University press, Cambridge, 1−704

Qin SF, Jia CZ, Tao SZ (2002) Some characteristics of oil and gas accumulation in the Kuqa Depression, Tarim Basin. Geol China 2:103−108

Shang XQ, Liu LF, Gao X, Jiang ZX, Liu GD (2012) Characteristics of hydrocarbon pathway system and transport model of the Yiqikelike structural belt in Kuqa Depression. J Daqing Pet Inst 36:25–30

Shi JX, Li BC, Fu JF, Liu DH, Peng PA (1987) Organic inclusions and their relation to oil and gas. Sci Sin (B) 3:318–326

Stasiuk LD, Snowdon LR (1997) Fluorescence micro-spectrometry of synthetic and natural hydrocarbon fluid inclusions: crude oil chemistry, density and application to petroleum migration. Appl Geochem 12:229–241

Tang HZ, Zhao JY, Gao G, Ma GF, Zhao LY, Yang ZM, Hu DD (2019) Geologically distributing relation of crude oils and source rocks in Ying'er Sag, Jiuquan Basin. Nat Gas Geosci 30:1590–1599

Tao SZ, Wang CY, Du JG, Liu L, Chen Z (2015) Geochemical application of tricyclic and tetracyclic terpanes biomarkers in crude oils of NW China. Mar Petrol Geol 67:460–467

Thanh HV, Lee KK (2022) 3D geo-cellular modeling for Oligocene reservoirs: a marginal field in offshore Vietnam. J Pet Explor Prod Technol 12:1–19

Thanh HV, Sugai Y, Nguele R, Sasaki K (2019) Integrated workflow in 3D geological model construction for evaluation of CO_2 storage capacity of a fractured basement reservoir in Cuu Long Basin. Vietnam Int J Greenhouse Gas Control 90:102826

Thanh HV, Sugai Y, Sasaki K (2020) Impact of a new geological modelling method on the enhancement of the CO_2 storage assessment of E sequence of Nam Vang field, offshore Vietnam. Energy Sources 42:1499–1512

Wang F, You M, Liu C, Zhang SC, Zhang B, Zhao M,Qin S, Zhao J (2000) Thermal maturation and hydrocarbon generation history of the Mesozoic source rocks in the Kuqa foreland region of the Tarim Basin. In: abstracts of the 8th Chinese National Meeting on Organic Geochemistry, Chin. Pet. Soc. Beijing. 55–57

Wang FY, Zhang SC, Zhang BM, Zhao MJ (1999) Organic maturity of mesozoic source rocks in kuqa depression, tarim basin. Xinjiang Pet Geol 20:221–224

Wang LS, Li C, Liu SW, Li H, Xu MJ, Yu DY, Jia CZ, Wei GQ (2005) Terrestrial heat flow distribution in Kuqa foreland basin, Tarim, NW China. Pet Explor Dev 4:79–83

Wei GQ, Jia CZ (1998) Structural charact erist ics and oil & gas of t hrust belt s in Tarim Basin. Acta Pet Sin 19:11–17

Wei HX, Huang WH, Luo HN, Li L, Shi LL, Wang ZT (2016) Faults characteristics and evolution in the eastern Kuqa Depression. Earth Sci 41:1074–1080

Wu H, Zhao MJ, Zhuo QG, Lu XS, Li WQ, Zeng F, Zhao AW (2016a) Palaeofluid evolution process in Well Block Tubei 1 in the Kuqa Depression, Tarim Basin. Nat Gas Ind 36:26–35

Wu H, Zhao MJ, Zhuo QG, Xu ZX, Bai DL, Zhou YZ, Zhang B, Wang L (2016b) Hydrocarbon accumulation process analysis of dina 2 condensate gasfield in Kuqa Depression. J Xi'an Pet Inst Nat Sci Ed 31:30–38

Xiao H, Li MJ, Yang Z, Zhu ZL (2019) Distribution patterns and geochemical implications of C 19–C23 tricyclic terpanes in source rocks and crude oils occurring in various depositional environments. Geochim 48:63–72

Zeng LB (2004) Characteristics and petroleum geological significance of Himalayan orogeny in Kuqa foreland basin. Oil Gas Geol 25:175–179

Zhang W, Xu ZP, Zhao FQ, Wu SJ, Huang C, Zhang XQ (2019) Structural deformation styles and tectonic evolution characteristics in eastern Kuqa Depression. Xinjiang Pet Geol 40:48–53

Zhao JZ, Dai JX (2002) Accumulation timing and history of kuche petroleum system. Tarim Basin Acta Sedimentol Sin 20:314–319

Zhao MJ, Lu SF (2003) Two periods of reservoir forming and their significance for hydrocarbon distribution in Kuqa Depression. Acta Pet Sin 24:16–25

Zhao MJ, Song Y, Pan WQ, Han JF, Liu SB, Qin SF (2004) The overall approach of hydrocarbon filling periods and process in sedimentary basins. Adv Earth Sci 19:939–946

Zhao MJ, Xiao ZY, Peng Y, Li M (1998) Geochemistry of oils from coal and from the shale in coal measure strata. Petrol Explor Dev 25:8–11

Zhao MJ, Zhang BM (2002) Source rocks for a giant gas-accumulating area in the kuqa foreland depression. Sci Geol Sin 37:35–44

Zhao SF, Chen W, Zhou L, Zhou P, Zhang J (2019) Characteristics of fluid inclusions and implications for the timing of hydrocarbon accumulation in the cretaceous reservoirs, Kelasu Thrust Belt, Tarim Basin. China Mar Petrol Geol 99:473–487

Zhu GY, Yang HJ, Zhang B, Su J, Chen L, Lu YH, Liu XW (2012) The geological feature and origin of Dina 2 large gas field in Kuqa Depression, Tarim Basin. Acta Petrol Sin 28:2479–2492